NASA
Technical
Paper
3302

February 1993

Longitudinal-Control Design Approach for High-Angle-of-Attack Aircraft

Aaron J. Ostroff
and Melissa S. Proffitt

NASA

NASA Technical Paper 3302

1993

Longitudinal-Control Design Approach for High-Angle-of-Attack Aircraft

Aaron J. Ostroff
Langley Research Center
Hampton, Virginia

Melissa S. Proffitt
Lockheed Engineering & Sciences Company
Hampton, Virginia

NASA
National Aeronautics and Space Administration
Office of Management
Scientific and Technical Information Program

Contents

Summary

This paper describes a control synthesis methodology that emphasizes a variable-gain output feedback technique that is applied to the longitudinal channel of a high-angle-of-attack aircraft. The aircraft is a modified F/A-18 aircraft with thrust-vectored controls. The flight regime covers a range up to a Mach number of 0.7; an altitude range from 15 000 to 35 000 ft; and an angle-of-attack (α) range up to 70°, which is deep into the poststall region. A brief overview is given of the variable-gain mathematical formulation as well as a description of the discrete control structure used for the feedback controller. This paper also presents an approximate design procedure with relationships for the optimal weights for the selected feedback control structure. These weights are selected to meet control design guidelines for high-α flight controls. Those guidelines that apply to the longitudinal-control design are also summarized. A unique approach is presented for the feed-forward command generator to obtain smooth transitions between load factor and α commands. Finally, representative linear analysis results and nonlinear batch simulation results are provided.

Results from linear single-loop stability and multiloop μ analyses show a high degree of robustness. A sensitivity analysis of four stability derivatives shows that the minimum singular values for 38 out of 39 design cases are above 1, which indicates excellent robustness. Nonlinear batch simulations show good agility for both pitch-up and pitch-down maneuvers and good α regulation.

Introduction

In recent years, researchers have investigated the feasibility of flight at a high angle of attack (α) in the poststall regime. Operation in this flight regime enables the aircraft to decrease speed rapidly and execute quick turns within a small turning radius so that the pilot can position the aircraft for the first shot at a target. High-α flight can be accomplished with thrust-vectored controls to augment the more classical aerodynamic control surfaces that lose effectiveness in the stall region. Control methodologies must now accommodate this highly nonlinear flight regime in addition to traditional ones.

The traditional approach for gain scheduling has been to develop individual, constant-gain feedback control laws at many operating points over the flight regime. These feedback gains are combined with a curve-fit technique (interpolation, straight line approximation, or a least squares fit) to create a gain schedule for the final control gains. Several schedules are often combined when more than one independent variable is involved. In a modern control design where a matrix of feedback gains is generated, traditional gain scheduling may cause the loss of performance characteristics and possibly stability in sensitive high-order plants (mathematical representation of aircraft). These control characteristic changes can occur if the actual gains are significantly different from the design gains.

Recently, the variable-gain output feedback technique was developed (refs. 1 and 2). In this approach, the gain schedule is optimally generated internal to the design algorithm. Variable gain is an integrated design approach in which all design operating conditions are handled simultaneously, thereby creating a more efficient design process. All operating points that are considered in the integrated design are guaranteed to be stable. The developed controller is nonlinear; however, linear design and analysis techniques are used. Thus, the designer can rely upon the wealth of previously developed techniques. This paper describes the application of variable-gain methodology to the high-α aircraft. Results of the design validation simulations are also presented.

Variable-gain output feedback was originally applied to reconfigurable aircraft flight control technology (ref. 3). In that successful application, feedback gains were calculated as a function of control effector failures. A second application involved a high-α, high-performance aircraft in which feedback gains varied with flight conditions (ref. 4). That work serves as a feasibility precursor to the control design described here.

The variable-gain approach is applied to a proportional integral filter (PIF) discrete control structure (refs. 5 and 6) with a command-generator tracker (CGT) feed-forward path (refs. 6 and 7). The PIF control structure used here is a direct digital formulation that accommodates the computational time lag from rate to position commands. Control of the rate command can ensure that actuators are not overdriven. With the CGT feed-forward structure, the pilot's command changes go directly to the rate command signal, which results in faster transient response. The PIF-CGT is part of the feedback controller, which derives its signal from a feed-forward command generator (FFCG). The FFCG generates commands that are interpreted by the feedback controller based upon pilot stick commands. The FFCG includes a unique approach for integration and smooth transition between two command modes—the load-factor command that applies at high speeds and the α command that applies at high α and low speeds.

This paper commences with an overview of the mathematical formulation for the variable-gain methodology and the PIF-CGT formulation. The overview is followed by a description of the appropriate control design guidelines and the high-α aircraft model. Subsections contain descriptions of the feedback controller and the FFCG as well as the PIF-CGT controller and the FFCG implementation. An approximate design procedure is included for selection of the initial optimal weights for the feedback controller; also provided are the relationships necessary to change these weights. The last subsection contains the design procedure for the FFCG.

Results are included for the linear analysis and nonlinear batch simulation. Linear analysis results include both gain and phase margins and a frequency response for a combined model composed of rigid body and servoelastic data. Nonlinear batch simulation results show closed-loop agility for both pitch-up and pitch-down time responses and α regulation during 360° rolls. All time responses are compared with design guidelines.

Nomenclature

$\mathbf{A}_p$	continuous plant state matrix
$\mathbf{A}_{11}, \mathbf{A}_{12}, \mathbf{A}_{21}, \mathbf{A}_{22}$	feed-forward coefficient matrices
$\mathbf{B}_p$	continuous plant control matrix
$\mathbf{B}_w$	process noise matrix
$\mathbf{C}$	plant and controller state to output matrix
C_i	steady-state normalized coefficients, $i = 1$, 2, or 3
$\mathbf{C}_p$	plant state to output matrix
C_1, C_2, C_3	steady-state normalized coefficients for α, q, and n_z
$\mathbf{D}_p$	plant control to output matrix
E	expectation operator
$\mathbf{E}1$	command-generator tracker feed-forward gain

f	scalar-weighting matrix for cost function
g	acceleration due to gravity, ft/sec^2
$\mathbf{H}_{zx}$	matrix that relates plant states to integrator states
$\mathbf{H}_{zy}$	matrix that relates measurements to integrator states
$\mathbf{I}$	identity matrix
J	global cost
$\overline{J}$	local cost
$\mathbf{K}$	feedback gain matrix
$\mathbf{K}_i, \mathbf{K}_0$	variable-gain feedback matrix partitions
$\mathbf{K}_n$	proportional feedback gain matrix for n_z, deg/sec/g
$\mathbf{K}_q$	proportional feedback gain matrix for q
$\mathbf{K}_u$	control filter feedback gain matrix, sec^{-1}
$\mathbf{K}_y$	proportional feedback gain matrix
$\mathbf{K}_z$	integrator feedback gain matrix
$\mathbf{K}_\alpha$	proportional feedback gain matrix for α, sec^{-1}
M	individual operating points
N	integer for series summation
n_z	load factor, g
$n_{z,c}$	load-factor command, g
$n_{zo,c}$	load-factor command trim, g
$\mathbf{P}_{ij}$	partitions of covariance matrix where ij represents all nine combinations representing x, u, and z components
P_s	static pressure, lb/ft^2
p	gain-schedule parameter
p_s	stability-axis roll rate, deg/sec
$\mathbf{Q}$	discrete-state weighting matrix
Q_c	impact pressure, lb/ft^2
Q_n	continuous weighting for n_z
Q_q	continuous weighting for q
Q_u	continuous weighting for control filter
$\mathbf{Q}_y$	continuous weighting matrix for outputs
Q_z	continuous weighting for integrator
Q_α	continuous weighting for α
q	pitch rate, deg/sec

$\dot{q}$	pitch acceleration, deg/sec^2
q_c	pitch-rate command, deg/sec
$\mathbf{R}$	continuous-control weighting matrix
$\mathbf{u}_c$	controller input command vector
$\mathbf{u}_p$	plant control input vector
$\dot{\mathbf{u}}_p$	time derivative of vector $\mathbf{u}_p$
V	total airspeed, ft/sec
$\mathbf{v}_c$	rate command vector, deg/sec
$\mathbf{w}$	plant and controller process noise vector
$\mathbf{w}_p$	plant process noise vector
$X(\ )$	arguments of variable X
$\mathbf{x}$	plant and controller state vector
$\mathbf{x}_p$	plant state vector
$\dot{\mathbf{x}}_p$	first derivative of plant state vector
$\mathbf{y}$	plant and controller output vector
$\mathbf{y}_c$	controller output vector, deg
y_{cmd}	command from feed-forward command generator
$\mathbf{y}_p$	plant output vector
$\mathbf{y}_{p,ss}$	normalized vector of C_i coefficients
$\mathbf{y}_u$	output vectors for controller position command state
$\mathbf{y}_z$	output vectors for integrator state
$\mathbf{z}$	integrator state vector or z-transform variable
$\dot{\mathbf{z}}$	time derivative of integrator state vector $\mathbf{z}$
α	angle of attack, deg
α_c	angle-of-attack command, deg
α_{oc}	angle-of-attack command trim, deg
β	sideslip angle, rad
$\mathbf{\Gamma}$	discrete plant and controller control matrix
$\mathbf{\Gamma}_p$	discrete plant control matrix
$\mathbf{\Gamma}_w$	discrete plant and controller process noise matrix
γ_w	discrete plant process noise
$\Delta n_{z,c}$	perturbation in $n_{z,c}$, g
Δ_{qc}	perturbation in q_c, deg/sec
ΔT	sampling period, sec
Δy	error signal to integrator

$\Delta\alpha_c$	perturbation in α_c, deg
δ_s	stabilator
δ_{sc}	stabilator command, deg
δ_{sp}	pilot stick command, in.
δ_v	pitch thrust-vectored control
δ_{vc}	pitch thrust-vectored command, deg
ζ	damping ratio
$\boldsymbol{\eta}$	discrete plant and controller measurement noise vector
$\boldsymbol{\eta}_p$	plant measurement noise vector
θ	pitch attitude, deg
μ	structured singular value
ν	measured variables used to calculate p
$\boldsymbol{\Phi}$	discrete plant and controller state transition matrix
$\boldsymbol{\Phi}_p$	discrete plant-state transition matrix
ϕ	bank angle, rad
ω_c	crossover frequency, rad/sec
ω_n	natural frequency, rad/sec
Subscripts:	
c	controller or command
i, j	series integers
k	coefficient for sampling sequence
p	plant
Superscripts:	
T	transpose
-1	inverse
Abbreviations:	
CGT	command-generator tracker
FFCG	feed-forward command generator
PI	proportional integral
PIF	proportional integral filter

Mathematical Formulation Overview

The control synthesis approach for variable-gain optimal output feedback is applied to a PIF discrete control structure. In this section is a review of the formulation for the PIF design with a single model; then, based upon that explanation, we show how to apply the variable-gain synthesis technique. Finally, the CGT formulation is reviewed. Please note that in the formulation that follows, many of the symbols defined as vectors are later used as scalars in the example problem.

PIF Formulation With Variable-Gain Application

The dynamic process for the plant is represented by

$$\left.\begin{aligned} \dot{\mathbf{x}}_p &= \mathbf{A}_p\mathbf{x}_p + \mathbf{B}_p\mathbf{u}_p + \mathbf{B}_w\mathbf{w}_p \\ \mathbf{y}_p &= \mathbf{C}_p\mathbf{x}_p + \boldsymbol{\eta}_p \end{aligned}\right\} \tag{1}$$

where $\mathbf{x}_p$, $\mathbf{y}_p$, and $\mathbf{u}_p$ are the state, output, and control vectors for the plant; $\mathbf{w}_p$ and $\boldsymbol{\eta}_p$ are process and measurement noise vectors; and $\mathbf{A}_p$, $\mathbf{B}_p$, and $\mathbf{C}_p$ are the plant state, control, and output matrices and $\mathbf{B}_w$ is the process noise matrix. Each noise process is assumed to be white with zero mean; the processes are uncorrelated.

The PIF controller is a rate-command system composed of a proportional integral (PI) section and a filter section (see fig. 1). The filter is constructed by feeding the control position command $\mathbf{y}_c$ back to the rate command $\mathbf{v}_c$ through a gain matrix. If $\mathbf{y}_c$ is connected to $\mathbf{u}_p$, the equations for the open-loop PIF model are

$$\dot{\mathbf{u}}_p = \mathbf{v}_c \tag{2}$$

$$\dot{\mathbf{z}} = \mathbf{H}_{zy}\mathbf{y}_p = \mathbf{H}_{zx}\mathbf{x}_p \tag{3}$$

where $\mathbf{v}_c$ is the rate command vector for the controller (control feedback point), $\mathbf{z}$ is the vector for the integrator state, and $\mathbf{H}_{zy}$ and $\mathbf{H}_{zx}$ are matrices that select the measurements and states to be integrated. The controller states in equations (2) and (3) are also outputs used in the design process.

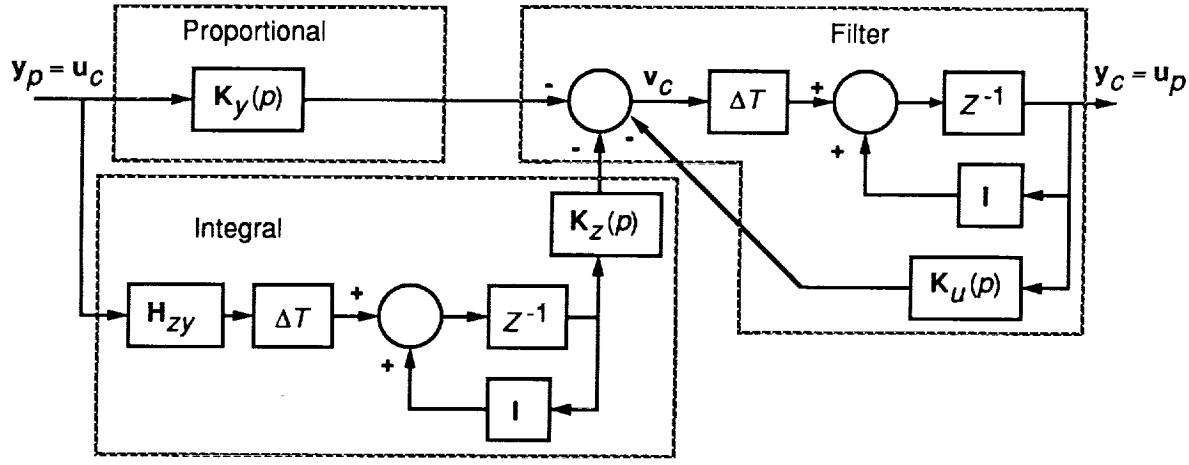

Figure 1. PIF control structure.

The design approach is to augment the PIF equations to the plant equation and discretize to form

$$\begin{Bmatrix} \mathbf{x}_p \\ \mathbf{u}_p \\ \mathbf{z} \end{Bmatrix}_{k+1} = \begin{bmatrix} \boldsymbol{\Phi}_p & \boldsymbol{\Gamma}_p & 0 \\ 0 & \mathbf{I} & 0 \\ (\Delta T)\,\mathbf{H}_{zx} & 0 & I \end{bmatrix} \begin{Bmatrix} \mathbf{x}_p \\ \mathbf{u}_p \\ \mathbf{z} \end{Bmatrix}_k + \begin{bmatrix} 0 \\ (\Delta T)\,\mathbf{I} \\ 0 \end{bmatrix} \mathbf{v}_{c,k} + \begin{bmatrix} \gamma_w \\ 0 \\ 0 \end{bmatrix} \mathbf{w}_k \tag{4a}$$

$$\begin{Bmatrix} \mathbf{y}_p \\ \mathbf{y}_u \\ \mathbf{y}_z \end{Bmatrix}_k = \begin{bmatrix} \mathbf{C}_p & 0 & 0 \\ 0 & \mathbf{I} & 0 \\ 0 & 0 & \mathbf{I} \end{bmatrix} \begin{Bmatrix} \mathbf{x}_p \\ \mathbf{u}_p \\ \mathbf{z} \end{Bmatrix}_k + \begin{Bmatrix} \boldsymbol{\eta}_p \\ 0 \\ 0 \end{Bmatrix}_k \tag{4b}$$

where $\boldsymbol{\Phi}_p$, $\boldsymbol{\Gamma}_p$, and γ_w are the discrete matrices corresponding to $\mathbf{A}_p$, $\mathbf{B}_p$, and $\mathbf{B}_w$; $\mathbf{y}_u$ and $\mathbf{y}_z$ are output vectors for the control command and integrator, respectively; ΔT is the discrete

sampling period; subscript k is an integer representing the present time; and the other subscripts are the same as previously defined. Note that $\mathbf{y}_u$ is equivalent to $\mathbf{y}_c$. The control $\mathbf{v}_{c,k}$ is related to the outputs by the feedback gain matrix as

$$\mathbf{v}_{c,k} = -\left[\mathbf{K}_y \quad \mathbf{K}_u \quad \mathbf{K}_z\right] \left\{ \begin{array}{c} \mathbf{y}_p \\ \mathbf{y}_u \\ \mathbf{y}_z \end{array} \right\}_k \tag{5}$$

Equations (4a) and (4b) represent the system at a single operating point; however, design for a comprehensive flight envelope requires many operating points. The variable-gain synthesis approach is effective when many design conditions are integrated and operated upon simultaneously. The resulting feedback gains are functions of the a priori gain schedule parameters that are chosen. The discrete state and output equations (eqs. (4) and (5)) can be rewritten in general form and in terms of arguments that represent scalar parameters p and sampling time k as

$$\mathbf{x}(p, k+1) = \mathbf{\Phi}(p)\,\mathbf{x}(p, k) + \mathbf{\Gamma}(p)\,\mathbf{v}_c(p, k) + \mathbf{\Gamma}_w \mathbf{w}(p, k) \tag{6}$$

$$\mathbf{y}(p, k) = \mathbf{C}(p)\,\mathbf{x}(p, k) + \boldsymbol{\eta}(p, k) \tag{7}$$

$$\mathbf{v}_c(p, k) = -\mathbf{K}(p)\,\mathbf{y}(p, k) \tag{8}$$

Each operating point described in equations (6) and (7) has a cost function $\overline{J}[p, \mathbf{K}(p)]$ that is quadratic in states and controls. First, the cost function is formulated in the continuous domain, then the function is transformed into an equivalent discrete cost as

$$\overline{J}[p, \mathbf{K}(p)] = \lim_{N \to \infty} \frac{1}{2(N+1)} \sum_{k=0}^{N} E\left[\mathbf{x}(p, k+1)^T \mathbf{Q}(p)\,\mathbf{x}(p, k+1) + \mathbf{v}_c(p, k)^T \mathbf{R}(p)\,\mathbf{v}_c(p, k)\right] \tag{9}$$

where $\mathbf{K}(p)$ is the feedback gain matrix and $\mathbf{Q}(p)$ and $\mathbf{R}(p)$ are the discrete weighting matrices. For simplicity, the cross term between the state and control vectors is not included in this paper, although the term is in the design algorithm. The main objective is to minimize a global cost $J(\mathbf{K})$, expressed by

$$J(\mathbf{K}) = \sum_{j=1}^{M} f_j \overline{J}_j[p, \mathbf{K}(p)] \qquad (f_j \geq 0) \tag{10}$$

where the local costs are summed and weighted by f_j to assign relative priorities to the M individual operating points.

The feedback gain matrix in equation (8) has a linear, functional relationship with p and contains both constant- and variable-gain parts that are implemented as

$$\mathbf{K}(p) = \mathbf{K}_0 + \sum_{i=1}^{q} p_i(\nu_i)\,\mathbf{K}_i \tag{11}$$

where the variable ν_i represents some measured variable that the designer selects for the gain schedule parameter. The relationship between the p_i and ν_i may be either linear or nonlinear.

First, the feedback gain matrix $\mathbf{K}(p)$ is partitioned into proportional gains $\mathbf{K}_y(p)$, integral gains $\mathbf{K}_z(p)$, and filter gains $\mathbf{K}_u(p)$ as

$$\mathbf{K}(p) = \left[\mathbf{K}_y(p) \quad \mathbf{K}_z(p) \quad \mathbf{K}_u(p)\right] \tag{12}$$

Next, the gains are incorporated into the PIF control structure, as shown schematically in figure 1. The sum of the PI feedbacks goes to a first-order, low-pass filter before $\mathbf{y}_c$ is generated. This sum of all feedback signals is $\mathbf{v}_c$, which is the rate command and the control signal for the PIF design (eqs. (4a) and (4b)). Control of the rate command ensures that actuators are not overdriven. The transfer function $\mathbf{v}_c$ to $\mathbf{y}_c$ is an integration and accommodates one computational time step during the design phase (fig. 1 and eqs. (2) and (4)).

CGT Formulation

The CGT is based on the theory that the integrated plant outputs can track the linearized, command model outputs (refs. 5 to 7). If the plant does not have a transmission zero at zero frequency, then the first step is to invert the plant to form coefficient matrices $\mathbf{A}_{ij}$. Thus,

$$\begin{bmatrix} \mathbf{A}_{11} & \mathbf{A}_{12} \\ \mathbf{A}_{21} & \mathbf{A}_{22} \end{bmatrix} = \begin{bmatrix} \mathbf{\Phi}_p & \mathbf{\Gamma}_p \\ \mathbf{H}_{zx} & 0 \end{bmatrix}^{-1} \tag{13}$$

where a single plant model is used for simplicity. If the output of the command model equals the input, then $\mathbf{A}_{22}$ is the only coefficient of interest. The solution for the feed-forward gain $\mathbf{E1}$ can be calculated as

$$\mathbf{E1} = \mathbf{K}_y\mathbf{A}_{12} + \left(\mathbf{K}_u - \mathbf{K}_z\mathbf{P}_{zz}^{-1}\mathbf{P}_{uz}^T\right)\mathbf{A}_{22} \tag{14}$$

where $\mathbf{P}_{zz}$ and $\mathbf{P}_{uz}$ are partitions from the matrix solution $\mathbf{P}$ to the output feedback cost equation (eq. (32) in ref. 2), shown here as

$$\mathbf{P} = \begin{bmatrix} \mathbf{P}_{xx} & \mathbf{P}_{xu} & \mathbf{P}_{xz} \\ \mathbf{P}_{xu}^T & \mathbf{P}_{uu} & \mathbf{P}_{uz} \\ \mathbf{P}_{xz} & \mathbf{P}_{uz}^T & \mathbf{P}_{zz} \end{bmatrix} \tag{15}$$

In equation (15), the subscripts x, u, and z correspond to the plant states, control position states, and integrator states, respectively. Equations (13) to (15) are solved for $\mathbf{E1}$ at each design condition.

Before the theory just presented can be applied, control design guidelines must be established. The following section provides a review of the design guidelines. Also in this section is a description of the high-α aircraft.

Guidelines

Several preliminary design guidelines were established to assist in the design effort. Many of these guidelines were developed through extensive piloted simulations. Although they are still being reviewed, these guidelines include linear criteria for flying qualities and robustness, large-amplitude criteria for agility and nonlinear coupling, and pilot-in-loop criteria for task-dependent agility and handling qualities. Those guidelines that apply to the longitudinal control system and the variable-gain control design approach are addressed in this paper. Other guidelines, such as pilot-related criteria, are used in real-time simulation and are not discussed here. Most of the guidelines that relate to agility are discussed in reference 8; those guidelines that relate to stability criteria and servoelastic attenuation are in reference 9.

Typical stability guidelines (ref. 9) include single-loop gain margins of 6 dB and phase margins of 45°. Structured, singular-value, multiloop margins should be evaluated; however, quantitative guidelines have not been established yet. Agility guidelines (ref. 8) include minimum pitch rate q and pitch acceleration $\dot{q}$, which are criteria for pitch-up and pitch-down maneuvers at an altitude

of 25 000 ft. For example, the minimum $\dot{q}$ and q criteria for a full-aft pitch stick command are 96 deg/sec^2 and 55 deg/sec, respectively, starting from a $1g$ trim at $\alpha = 5°$ and the throttle commanded to full afterburner. The maximum $\dot{q}$ should be obtained within 1 sec from the onset of the pitch stick command, and the maximum q should be achieved within 1.75 sec. The tactically desirable nose-down guidelines for $\dot{q}$ and q are -14.5 deg/sec^2 and -24 deg/sec, respectively. When starting from a 60° trim, recovery to 10° should occur within 7 sec for safety considerations.

During roll coordination tasks with full lateral stick, the α-regulation guideline (ref. 8) is 6° for a 90° roll about the velocity vector; the guideline is 10° for a full 360° roll. Load factor n_z excursions should not exceed $0.5g$ in either case.

A final design guideline relates to structural frequency attenuation (ref. 9) of all servoelastic modes by at least 8 dB (gain of 0.25).

Aircraft Model

The mathematical model is representative of an F/A-18 class of aircraft that has been modified for thrust-vectored control. For this study, the aircraft has a gross weight of approximately 35 765 lb, a wingspan of 40 ft, and a length of 56 ft. Controls include two afterburner engines and the following aerodynamic control surfaces: horizontal stabilators; full-span, leading-edge flaps; trailing-edge flaps; ailerons; and twin vertical stabilizers. In addition, pitch and yaw thrust-vectored controls have been added for both longitudinal and lateral-directional maneuvers.

A longitudinal controller design was used here. (See fig. 2 for the main components of the longitudinal aircraft model used in the design and linear analysis and for the number of states.) The comprehensive aircraft model contains a series of models representing actuator dynamics, airplane longitudinal dynamics, and sensor and filter dynamics. Four states are used for the longitudinal equations of motion: total airspeed V, α, pitch rate q, and pitch attitude θ. The actuator dynamics portion is represented by unity gain with a fourth-order model for the stabilator and a second-order model for thrust-vectored control. The result is six states. The natural frequency and damping ratio combinations (ω_n, ζ) are (36.4, 0.41) and (105.0, 0.59) for stabilator δ_s and (75.0, 0.59) for pitch thrust-vectored control δ_v. The unit for ω_n is radians per second.

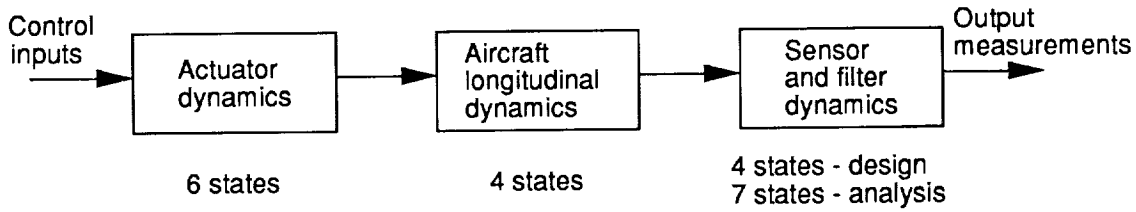

Figure 2. Longitudinal aircraft model.

Three measurements—α, q, and n_z—are used in the design. These measurements are modified by both sensor and antialiasing filter dynamics that are included in the block-labeled filters. Only the sensor dynamics for the α probe is relevant here because that probe is modeled by a first-order response with a bandwidth of 14 rad/sec. The (ω_n, ζ) combinations for each of the three antialiasing filters for the α, q, and n_z measurement order are (209.0, 0.74), (78.5, 0.89), and (200.0, 0.89). Six states represent the three antialiasing filters and one state represents the α probe; thus, seven states are used in the analysis. Because the antialiasing filter in the q measurement loop is the filter of interest, the design model includes two states for this filter.

These two states, added to one state for the α probe and one for approximation of the n_z filter, equate to four states.

Controller Design

In the example design, some of the symbols that have been shown as boldface (vector or matrix) will now be shown in italicized form for a scalar quantity. The two main parts of the controller that are illustrated in figure 3 are the FFCG and the feedback controller. The FFCG transforms the pilot stick command into an equivalent command y_{cmd} that can be interpreted by the feedback controller. The controller has two command modes (each with its own stick sensitivity): one for load factor n_z, which generally applies at high-speed flight; the other for α, which generally applies at low-speed, high-α flight. The FFCG must select one of the command modes and make a smooth transition from one to the other. The feedback controller must maneuver the aircraft agilely to orientations defined by y_{cmd} and regulate outputs about these new set points. In addition, the feedback controller must be robust to changes in plant parameters and must attenuate disturbances to avoid undesirable responses in the control loop.

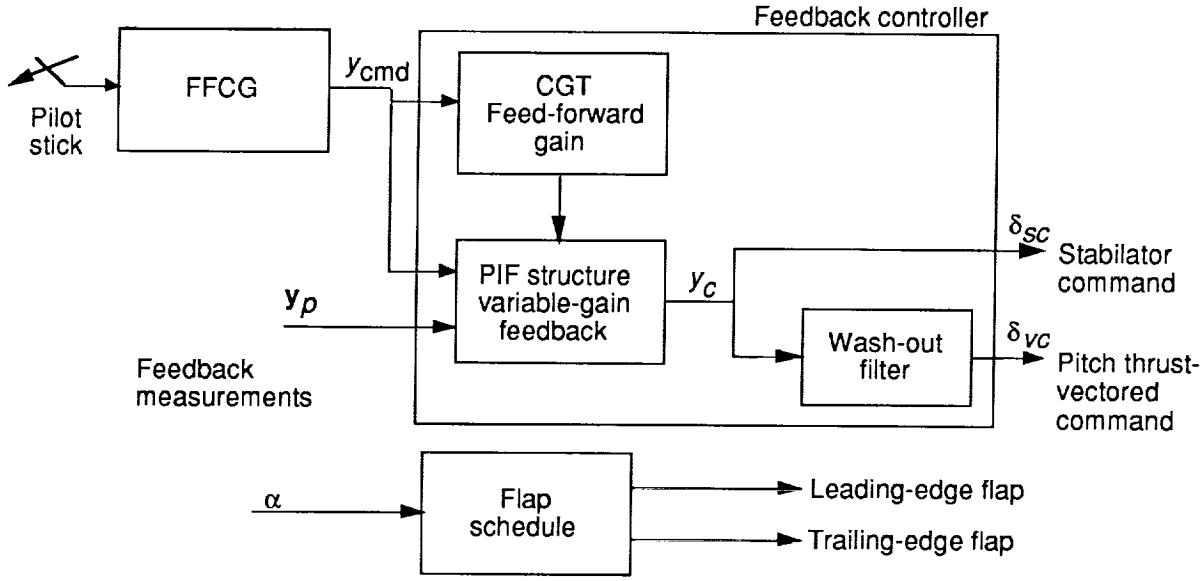

Figure 3. Overall controller configuration.

The control command output from the feedback controller (PIF structure) consists of the stabilator command δ_{sc} and the input to a limited wash-out filter. This filter maintains the pitch thrust-vectored control δ_{vc} at a neutral position during most flight conditions to keep the thrust-vectored vanes from overheating. The δ_{vc} control assists during transient maneuvers and becomes the main control when δ_s saturates.

One other key component of the control system is the flap schedule controller. Both leading- and trailing-edge flaps are driven by a flap schedule that is mainly a function of α and is gain scheduled with other air data parameters. This gain schedule is the same as the one being used on the F/A-18 aircraft.

The feedback controller implementation used for the high-α design is shown in figure 4. In this incremental approach, $\mathbf{K}_y(p)$ multiplies the incremental change in $\mathbf{y}_p$, $K_z(p)$ multiplies the difference between the sum of the measured feedbacks and y_{cmd} (in this example, y_{cmd} has only one value), and $K_u(p)$ is incorporated into the discrete filter loop. One advantage of this

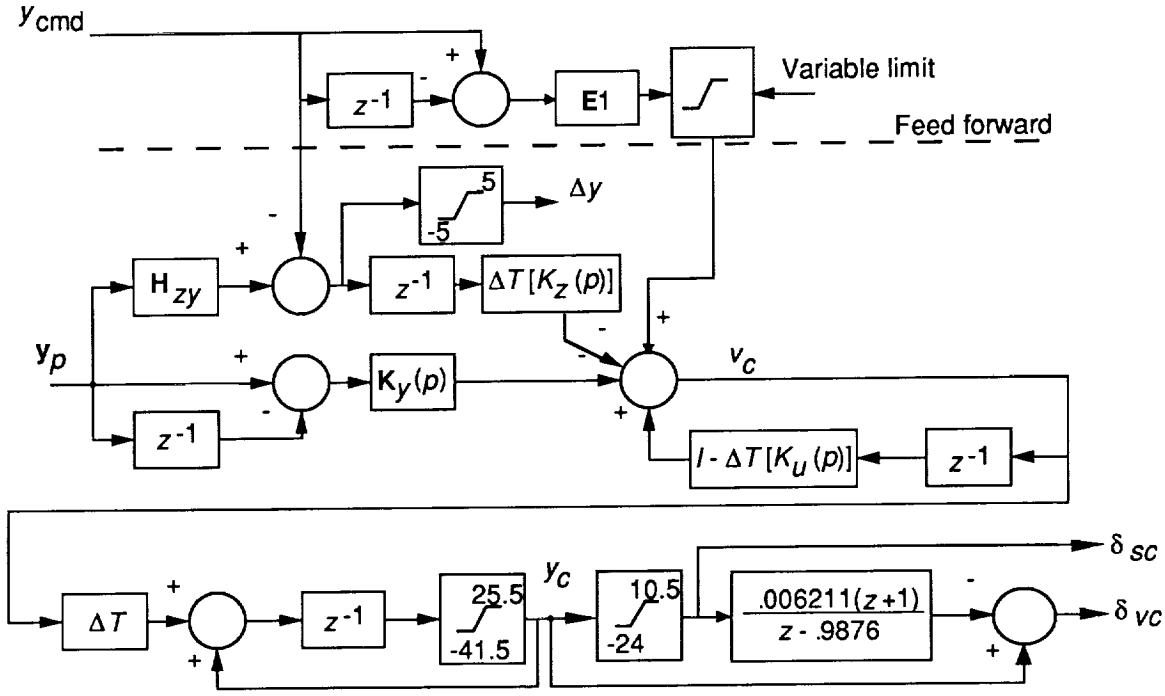

Figure 4. Feedback controller implementation.

incremental approach is that sensor biases are subtracted out in the proportional feedback loop. In the integrator loop, the pilot can move the pitch stick slightly to compensate for biases. Position limiters are incorporated to prevent windup in the rate-to-position integrator. The discrete dynamics in the δ_{vc} actuator loop represents the Tustin transformation for a low-pass filter with a bandwidth of 1 rad/sec.

The feed-forward gain (**E1** in eq. (14)) is calculated from the CGT design approach for a step input. This gain, which varies continuously over the flight envelope, multiplies the incremental change in y_{cmd}. Gain **E1** is independent of the feed-forward gains in the FFCG, which is discussed later. The CGT feed-forward path allows changes in pilot commands to go directly to the rate command signal, which results in faster transient response.

Feedback Controller

Thirty-nine design conditions (table I) are used for the feedback controller: 14 conditions are at 15 000 ft, 13 conditions are at 25 000 ft, and 12 conditions are at 35 000 ft. Nineteen of the design conditions are at 1g (Earth axis) flight. The other cases are at various non-1g conditions. The parameters in table I are the design case, altitude, Mach number, α, n_z, and open-loop short period. Because n_z is along the z axis of the aircraft, the 1g trim cases are lower by the cosine of the pitch attitude (not shown). Most of the non-1g trim cases are at higher loads; however, design cases such as 13 and 14 are at lower load factors.

Variable-gain parameters. The variable-gain feedback shown in equation (11) is repeated here as

$$\mathbf{K}(p) = \mathbf{K}_0 + \sum_{i=1}^{6} p_i(\nu_i)\,\mathbf{K}_i \tag{16}$$

Table I. Design Conditions

Design case	Mach number	α, deg	n_z, g	Short period, rad/sec
Altitude of 15 000 ft				
1	0.70	2.52	1.00	2.70
2	.60	3.37	1.00	2.10
3	.49	5	1.00	1.40
4	.27	20	.94	.57
5	.21	35	.82	.54
6	.20	50	.80	.83
7	.22	65	.82	1.30
8	.70	20	6.30	1.70
9	.60	20	4.90	1.60
10	.60	35	6.90	1.70
11	.40	20	2.10	.97
12	.40	35	3.10	.97
13	.30	5	.37	.79
14	.10	45	.22	.35
Altitude of 25 000 ft				
15	0.70	3.58	1.00	2.10
16	.59	5	1.00	1.50
17	.33	20	.94	.63
18	.26	35	.88	.56
19	.26	50	.90	.90
20	.28	65	.92	1.30
21	.70	20	4.20	1.50
22	.60	20	3.20	1.40
23	.60	35	4.50	1.40
24	.40	20	1.40	.82
25	.40	35	2.00	.83
26	.30	5	.24	.64
27	.10	45	.14	.27
Altitude of 35 000 ft				
28	0.70	5.34	1.00	1.50
29	.60	7.24	.99	1.00
30	.41	20	.94	.70
31	.34	35	.94	.60
32	.34	50	.95	.94
33	.35	60	.95	1.60
34	.70	20	2.70	1.20
35	.60	20	2.00	1.20
36	.60	35	2.90	1.10
37	.40	5	.28	.66
38	.40	50	1.40	1.10
39	.20	45	.34	.53

where six gain schedule parameters $p_i(\nu_i)$ are used. These parameters are functions of α, impact pressure Q_c, and static pressure P_s. The $p_i(\nu_i)$ and their limits are

$$\left.\begin{aligned} p_1 &= 0.1\alpha && (1.5 \le \alpha \le 65) \\ p_2 &= 0.01Q_c && (10 \le Q_c \le 470) \\ p_3 &= 0.001P_s && (498 \le P_s \le 1200) \\ p_4 &= \frac{Q_c}{P_s} && (0.008 \le p_4 \le 0.4) \\ p_5 &= 0.1\alpha - 3.5 && (\alpha > 35) \\ &= 0 && (\alpha \le 35) \\ p_6 &= 0.01Q_c - 2.5 && (Q_c > 250) \\ &= 0 && (Q_c \le 250) \end{aligned}\right\} \tag{17}$$

The feedback gains change continuously with the measured variables and the function is smooth except at two points. The first four parameters cover the entire flight envelope; the last two parameters cover only portions of the envelope. Parameter p_5 is used only when α is 35° or greater, and parameter p_6 is used when Q_c is 250 lb/ft^2 or greater. Both p_5 and p_6 have lower limits of zero and are not differentiable at the breakpoints. When any value of ν_i exceeds the design limit, the variable is limited to the value shown in equation (17).

Design procedure. This section presents a description of the relationships between the weighting matrices, feedback gains, and design performance. It also provides a description of an approximate procedure for designing a multi-input, single-output PIF controller. Figure 1 graphically portrays the transfer function from $\mathbf{u}_c$ to y_c as

$$y_c(z) = \left[\frac{-\Delta T}{z - (1 - \Delta T K_u)}\right]\left(\mathbf{K}_y + \frac{\Delta T K_z \mathbf{H}_{zy}}{z - 1}\right)\mathbf{u}_c(z) \tag{18}$$

wherein the argument p has been dropped for simplicity. The first term (in brackets) represents the transfer function for the filter; the second term (in parentheses) represents the PI transfer function. The variables $\mathbf{K}_y$ and $\mathbf{H}_{zy}$ are row vectors, $\mathbf{u}_c$ is a column vector, K_u and K_z are scalars, and z is the z-transform variable. The proportional gain matrix can be partitioned into individual scalar gains as

$$\mathbf{K}_y = [\,K_\alpha \quad K_q \quad K_n\,] \tag{19}$$

where the gains correspond to the measurements for α, pitch rate q, and load factor n_z, respectively. In this section, $\mathbf{K}_y$ is the proportional gain. The relationship between the individual gains is discussed later. The row vector $\mathbf{H}_{zy}$ is selected as

$$\mathbf{H}_{zy} = [\,1 \quad 1 \quad 1\,] \tag{20}$$

so that the three output measurements are summed, then integrated.

In the following discussion, weights are referenced to the continuous domain. Feedback gains ($\mathbf{K}_y$, K_u, K_z) are adjusted by varying the corresponding output penalty weights $\mathbf{Q}_y$, Q_u, Q_z, and the control-rate penalty weight R in the quadratic cost function. Changes in gains are approximately related to changes in the square of the corresponding penalty weight. The output measurements are related to the states through the $\mathbf{C}$ matrix in equation (7). First, all weights

are implemented in the continuous domain; then, they are discretized to determine corresponding weights $\mathbf{Q}$ and R for the discrete cost function in equation (9).

The bandwidth and steady-state gain of the low-pass filter are related to the control feedback gain K_u. A decreased control-rate penalty R results in a higher value of K_u, a correspondingly higher bandwidth, and a lower filter gain. Additional filtering can be obtained if K_u is lowered, but with the disadvantage of increased phase lag. A trade-off must be made between bandwidth and phase lag. The control bandwidth also can be adjusted if the penalty weight Q_u is changed. When an adjustment to R has little effect on bandwidth, a change in Q_u seems to help (and vice versa).

Higher gains for $\mathbf{K}_y$ and K_z result from increases in the penalty $\mathbf{Q}_y$ for the output measurements and Q_z for the integrator. The higher gain for $\mathbf{K}_y$ results in a faster time response to external commands; the larger K_z results in smaller low-frequency errors. The relationship between $\mathbf{K}_y$ and K_z is important because these gains affect the phase lag of the PI section. Therefore, a reduction of the ratio of Q_z to $\mathbf{Q}_y$ also will reduce the phase lag.

A Nyquist test of equation (18) can be performed by moving z around the unit circle in the complex plane to evaluate whether the structural attenuation guideline is achieved. The attenuation guideline will be met if the singular value of the norm of $y_c(z)/u_c(z)$ for any one input has a gain of less than 1 (0 dB) at all modal frequencies because all the modes will have peaks of -8 dB or lower. The crossover frequency in the pitch-rate control channel is the most critical and should occur at a frequency below 75 rad/sec.

The approximate design procedure that is summarized below applies to all design models. The suggested weights are provided as a starting point and can be modified with the appropriate relationships. The results described later in this report indicate that this procedure apparently works well in the design process.

1. Set $Q_u = 1$ and adjust all other weights relative to this weight.

2. Fix the ratio of weights for the proportional measurements Q_α, Q_q, and Q_n. A rough guideline for magnitude is to set the norm of these weights $\|\mathbf{Q}_y\|$ inversely proportional to the square of the percentage of deviation error allowed. For example, if the deviation error is within 7 percent, $\|\mathbf{Q}_y\|$ should be approximately 200.

3. Select R to adjust the bandwidth of the filter loop. For example, select the bandwidth to be approximately three to five times the short-period frequency, then calculate R as the inverse of the square of the bandwidth.

4. Select the integrator weight Q_z as a function of desired system crossover frequency ω_c and adjust the ratio

$$\frac{3Q_z}{Q_\alpha + Q_q + Q_n} < \frac{\omega_c}{10} \tag{21}$$

   to reduce the phase lag of the PI loop and maintain good, low-frequency characteristics. The factor of 3 in the numerator is shown because all three proportional measurements are summed before integration. This approach yields a rough approximation that must be adjusted if any one loop has too much phase lag or poor low-frequency characteristics.

The selected weights are discretized and incorporated into the synthesis program. Various analyses are then performed (i.e., closed-loop eigenvalues and damping ratios, frequency responses, stability margin evaluations, and time responses); based upon the results, weights are corrected according to the relationships described in this section. Typical corrections might include adjustment of R or the ratio of weights in equation (21) to change phase margin, adjustment of Q_z to correct the low-frequency response, and adjustment of $\mathbf{Q}_y$ to modify time

response. An adjustment of Q_u (from step 1 in the procedure) should be made only as one of the last steps or if the adjustment of R has little effect on filter bandwidth. An increase in Q_u allows a trade-off of less agility but improved gain and phase margins.

Feed-forward command generator. The FFCG converts the pilot's stick command into an equivalent command y_{cmd} that can be interpreted by the feedback controller. The FFCG selects either an n_z ($n_{z,c}$) or α command mode (α_c) and makes a smooth transition between the two modes without additional work by the pilot. The basis for designing the FFCG is to start at the error signal Δy in the feedback controller (fig. 4) so that

$$\Delta y = \mathbf{H}_{zy}\mathbf{y}_p - y_{\text{cmd}} \tag{22}$$

and, because $\mathbf{H}_{zy}$ is a row vector of ones (eq. (20)), all three output measurements are considered. Expand equation (22) into components and assume that y_{cmd} consists of contributions from three sources. Thus,

$$\Delta y = (\alpha - \alpha_c) + (q - q_c) + (n_z - n_{z,c}) \tag{23}$$

where the subscript c represents the command. Each of the variables can be separated into a perturbation plus a trim. The perturbations in the commands are related by the coefficients C_1, C_2, and C_3 (to be determined) as

$$\frac{\Delta\alpha_c}{\Delta n_{z,c}} = \frac{C_1}{C_3} \qquad \frac{\Delta\alpha_c}{\Delta q_c} = \frac{C_1}{C_2} \qquad \frac{\Delta q_c}{\Delta n_{z,c}} = \frac{C_2}{C_3} \tag{24}$$

and are substituted into equation (23). Relate the command perturbations $\Delta\alpha_c$ and $\Delta n_{z,c}$ (Δq_c is not considered in this design) to Δy_{cmd} as

$$\Delta y_{\text{cmd}} = \frac{\sum_{i=1}^{3} C_i}{C_3} \qquad \Delta n_{z,c} = \frac{\sum_{i=1}^{3} C_i}{C_1}\Delta\alpha_c \tag{25}$$

Thus, y_{cmd} is the sum of Δy_{cmd} plus trims α_{oc} and $n_{zo,c}$.

The pilot's stick command δ_{sp} and the stick sensitivity function determine the perturbation commands $\Delta n_{z,c}$ and $\Delta\alpha_c$. The sensitivity equations include a perturbation plus a bias

$$n_{z,c} = 1.3\delta_{sp} \tag{26}$$

$$\alpha_c = 10\delta_{sp} + 20 \tag{27}$$

with the units in inches for δ_{sp}, g for n_z, and degrees for α. Normally, the bias in equation (26) would be 1; however, because $1g$ is subtracted internal to the n_z sensor, the bias command $n_{zo,c}$ must also be at $0g$. The bias for the α stick function is 20°. When all terms have been combined, the final equations for y_{cmd} are

$$y_{\text{cmd}} = \frac{\sum_{i=1}^{3} C_i}{C_3}\left(1.3\delta_{sp}\right) + \alpha_{oc} \tag{28a}$$

$$y_{\text{cmd}} = \frac{\sum_{i=1}^{3} C_i}{C_1}\left(10\delta_{sp}\right) + 20 \tag{28b}$$

where α_{oc} must be estimated.

Implementation of the FFCG is illustrated in figure 5. Selection of the command y_{cmd} is based upon choosing the solution that has the lowest absolute value biased at -5. The negative bias is incorporated to ensure that negative load factors can be commanded for small negative δ_{sp} deflections. For positive δ_{sp} stick deflections, transition can occur only when the two solutions are equal. When the stick deflection is negative, one positive solution and one negative solution can occur simultaneously. A jump condition is possible when the two solutions are of opposite sign. A lockout feature was added to the implementation to minimize this jump. When the FFCG is in the α mode, that mode cannot change if the impact pressure is less than 80 lb/ft^2 or if the δ_{sp} is negative.

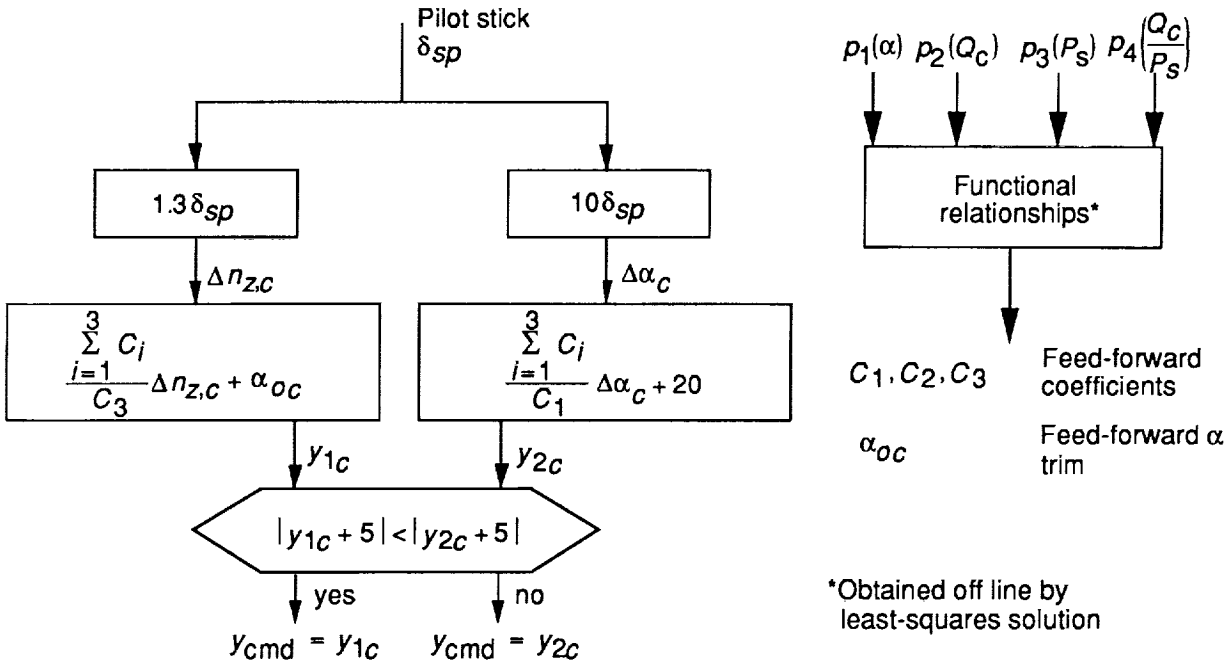

Figure 5. Block diagram of FFCG.

Coefficients C_1, C_2, and C_3 are determined for each design condition with a steady-state analysis of the open-loop short-period plant that was approximated. With an input of 1, the steady-state output is given as

$$\mathbf{y}_{p,ss} = -\mathbf{C}_p\mathbf{A}_p^{-1}\mathbf{B}_p + \mathbf{D}_p \tag{29}$$

where $\mathbf{y}_{p,ss}$ is a vector based upon one control and three measurements. The solution for the coefficients is

$$\begin{Bmatrix} C_1 \\ C_2 \\ C_3 \end{Bmatrix} = \frac{\mathbf{y}_{p,ss}}{\|\mathbf{y}_{p,ss}\|} \tag{30}$$

Evaluation of these coefficients shows that the solution from equation (28a) is dominant at high speed and low α, whereas the solution from equation (28b) is dominant at low speed and high α. Figure 6 contains a plot of these coefficients (solid line) calculated every 5° as a function of α for flight at 1g trim and an altitude of 25 000 ft. In practice, the goal is both to reduce the time required to calculate the C_i and to have smooth feed-forward commands. Because interpolation is time-consuming, a functional relationship was obtained from an off-line, least-squares solution. The selected inputs are the first four p_i (eq. (17)) used in the variable-gain feedback controller. Figure 6 contains the least-squares estimate for the C_i.

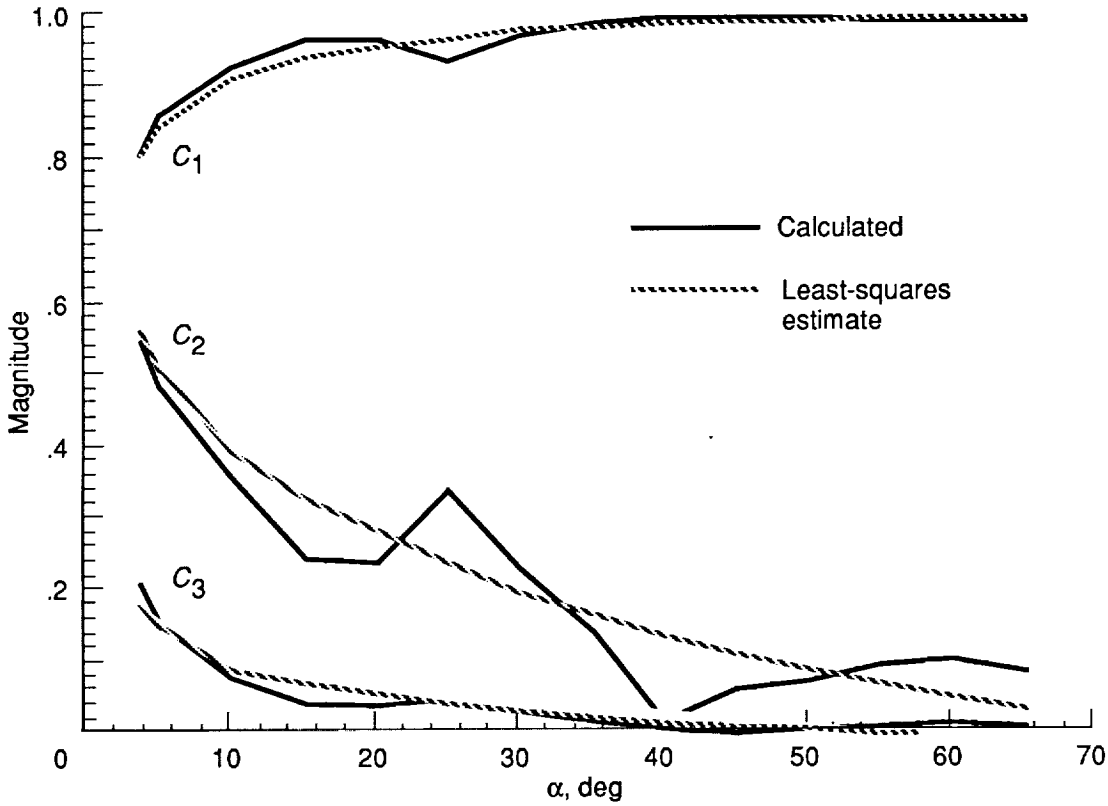

Figure 6. Feed-forward coefficients at $1g$ and 25 000 ft.

Equation (29) assumes a stable plant, which applies to most of the 39 design conditions. A few design cases in the stall region (high α) have short-period eigenvalues that are slightly unstable. However, C_1 is the dominant coefficient (near 1) and y_{cmd} (from eq. (28b)) is the dominant selection for the high-α cases; thus, the gain is essentially unchanged.

The next two sections present the linear analysis and nonlinear batch simulation results, respectively, for the longitudinal controller described above.

Results of Linear Analysis

This section presents results of the linear analyses. The main components of the aircraft model are described in the section "Aircraft Model" and are illustrated in figure 2. The design model has 14 states—6 for actuator dynamics, 4 for aircraft dynamics, and 4 for sensor and output filter dynamics.

Depending upon the type of linear analysis, the controller thrust-vectored wash-out filter can be incorporated either into the plant (which allows the input control loop to be broken at a single point rather than at two points) or the wash-out filter can be incorporated into the controller. The former configuration is used for single-loop gain and phase margins. The latter configuration is used for servoelastic frequency response and sensitivity studies where separate controls must be maintained.

Gain and Phase Margins

Although the design included only 39 operating conditions with a maximum Mach number of 0.7, the stability margins were analyzed at 133 conditions ranging to a Mach number of 0.9. All test cases within the flight envelope met both a gain margin guideline of 6 dB and a phase

margin guideline of 45°. Except for several high-speed cases at 15 000 ft, all other test cases outside the flight envelope also met the guidelines. The nondesign cases were equally as robust to changes in gain and phase as the 39 design cases. That similar robustness between the design and the nondesign cases indicates that the controller is not tuned to specific design points. The results were similar for both the plant input and each output loop. The q-measurement loop is the critical path; gain and phase margins for this plant output loop were similar to those at the plant input.

μ Analysis

A μ analysis (ref. 10) for a multiplicative error was performed at the plant output with all three output loops opened. Of the 39 design conditions, the worst cases were at an α between 20° and 50°; within these cases, the lowest magnitude (inverse of the maximum singular value) occurred just below 0.5. This result indicates that a simultaneous complex change of at least 50 percent would be required to produce an unstable control system; this safety margin is considered satisfactory for flight conditions.

A μ analysis also was used to evaluate the sensitivity of the aircraft stability and control derivatives that affect the short-period mode (α and q time derivatives). In the analysis of the four stability derivatives for the 39 design cases, the minimum singular values (with one exception) were above 1 for the frequency range near the short period. The exception was at an α of 60° at 35 000 ft; the minimum singular value was 0.9. In this type of analysis the phugoid, which is not directly controlled, has the most sensitivity with minimums near 0.1. Other preliminary calculations with real μ analysis indicate that the phugoid may also have minimums above 1. All four control derivatives in the 39 design conditions registered minimums of at least 0.6. Although no concrete guidelines exist for this type of analysis, these minimums can be considered quite good.

Loop Transfer

To conduct a singular-value, loop transfer analysis, the control loop was opened first at the single plant input, then at the plant output. Because the analysis has only one control, the Bode response and the singular-value response were identical at the plant input. At both input and output locations, the crossover frequencies for all 39 design conditions ranged from 2.4 rad/sec to 9 rad/sec, with a slope of approximately 6 dB per octave. The highest crossover frequency occurred at the highest Mach number. The filter bandwidth in the PIF feedback controller was reduced (lower filter gain) at higher α to obtain lower crossover frequencies.

Servoelastic Frequency Response

The servoelastic analysis was conducted as an extension of the rigid-body analysis; however, the plant input was opened at two controls. First, a servoelastic modal model was paralleled with a series combination of the rigid body and actuator dynamics, then the new model was connected in series with the output filters. Analysis of both light and heavy airplanes shows that the open-loop, servoelastic transfer function from control input to q output (units of sec^{-1}) exhibits peaks of -20 dB at 75 rad/sec and -8 dB at 100 rad/sec. In addition, the transfer function from control input to n_z output (units of g/deg) exhibits peaks of -45 dB at 37 rad/sec, -38 dB at 50 rad/sec, and -33 dB at 100 rad/sec. For the 39 design cases, singular-value loop transfer analysis at the plant input and output locations showed that the structural mode at 100 rad/sec was attenuated to -20 dB. This rate of attenuation is significantly lower than the guideline of -8 dB.

Results of Nonlinear Batch Simulation

Several nonlinear batch simulations were conducted to evaluate pitch-up and pitch-down agility and α regulation during stability-axis rolls of 360°. Nonlinear compensation q_{comp} was added to the pitch-rate measurement to compensate for nonlinear effects of gravity and the kinematic term composed of stability-axis roll rate p_s and sideslip β. The derivation for the compensation equation is shown in the appendix. The final result is

$$q_{\text{comp}} = \frac{1839}{V}(\cos\theta\cos\phi\cos\alpha + \sin\theta\sin\alpha - 1) - p_s\beta \tag{31}$$

where θ and ϕ are the body-axis pitch attitude and bank angle, respectively. The feedback controller implementation (fig. 4), which includes the wash-out filter for the pitch thrust-vectored command, was incorporated into the batch simulation. A rigid-body dynamic model with six degrees of freedom was used for the aircraft equations of motion. The aerodynamic tables were generated from a wind tunnel-derived data base; the tables include a range of $-10°$ to 90° for α and a range of $\pm 20°$ for sideslip. Flex-rigid ratios were used to incorporate flexibility effects.

Pitch-Up Agility

The objective of this maneuver was to evaluate the pitch-up response (fig. 7) to a full-pitch stick input of 5 in. when trimmed at an altitude of 25 000 ft and a Mach number of 0.6. In particular, the α, q, and $\dot{q}$ responses were measured. The latter two responses were compared with design guidelines. To simulate the maneuver, maximum throttle was commanded at time equal to 0.01 sec; 2 sec later, after thrust had built up, the pitch stick was ramped to maximum within 0.3 sec to simulate the approximate response time of the pilot. The top plot in figure 7 shows α reaching 60° in less than 2 sec, then slowly climbing to 70° after a slight bobble. The sluggish response after the α reached 60° was caused by the saturated actuator commands. The thrust-vectored command came out of saturation at approximately 5.6 sec as the α slowly converged toward 70°, although the stabilator remained saturated. The pitch rate peaked at approximately 51 deg/sec (slightly under the desired guideline of 55 deg/sec), whereas the pitch acceleration was greater than the guideline of 96 deg/sec^2. The FFCG started in the n_z mode and made a smooth transition to the α mode at approximately 3 sec. Based on this smooth transition, the pilot is unlikely to detect the transition. The smooth time response also indicated good integration between the feedback and feed-forward controllers.

Pitch-Down Agility

The objective of this maneuver was to evaluate the response (fig. 8) to a full-forward pitch stick input of -2.5 in. starting from an α trim of 60° and at an altitude of 25 000 ft. The α decreased to 10° in approximately 2 sec and crossed 0° shortly thereafter. This response fell well within the safety guideline that specifies a decrease to 10° within 7 sec; an equivalent tactical guideline has not been developed. Similarly, both q and $\dot{q}$ were significantly greater than the tactical guidelines of -24 deg/sec and -14.3 deg/sec^2, respectively. Based on these results, the α response is well damped. The system remained in the α mode with the n_z mode locked out because the input stick command remained constant at a negative value.

Angle-of-Attack Regulation

The objective of this maneuver was to evaluate the α regulation during full-lateral stick stability-axis rolls. Figure 9 illustrates four α trim cases: 5°, 30°, 45°, and 60°. The dashed vertical lines denote the time in seconds for wind-axis bank angles of 180° and 360°. In all cases, the α regulation was considerably better than the $\pm 10°$ guideline for a 360° roll. At an α trim

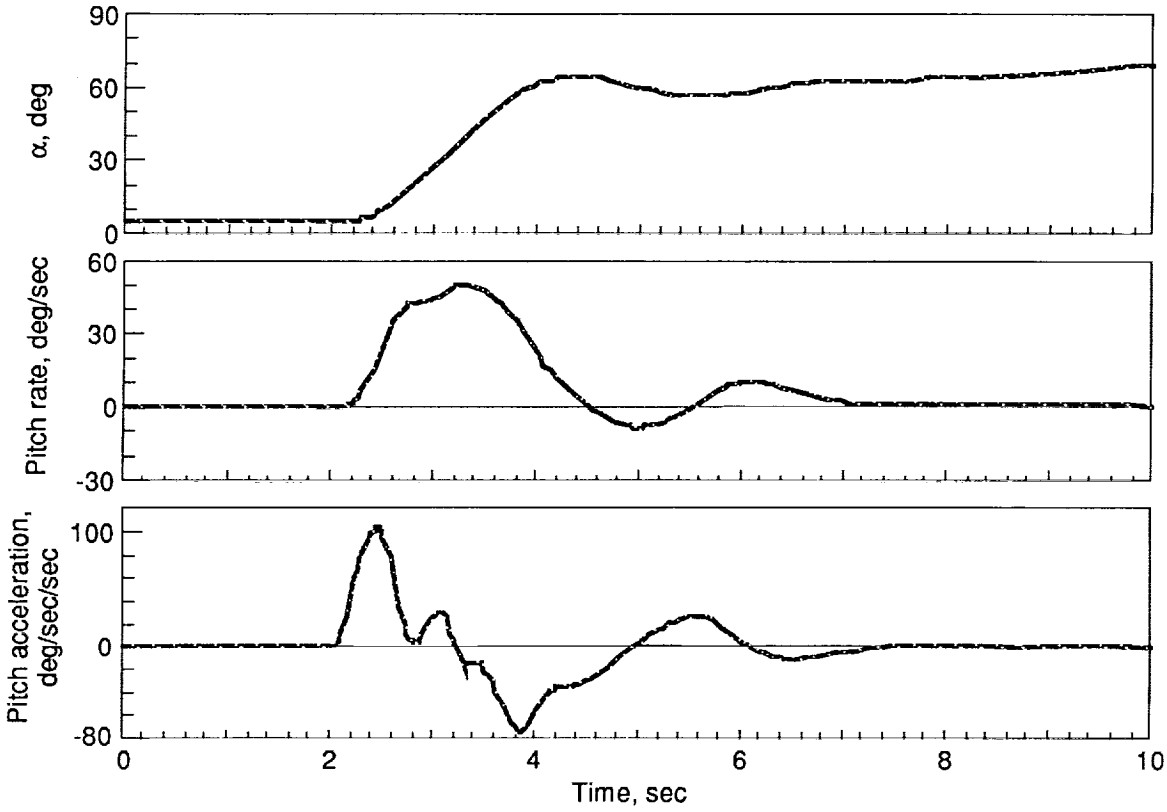

Figure 7. Pitch-up response, full stick at 25 000 ft.

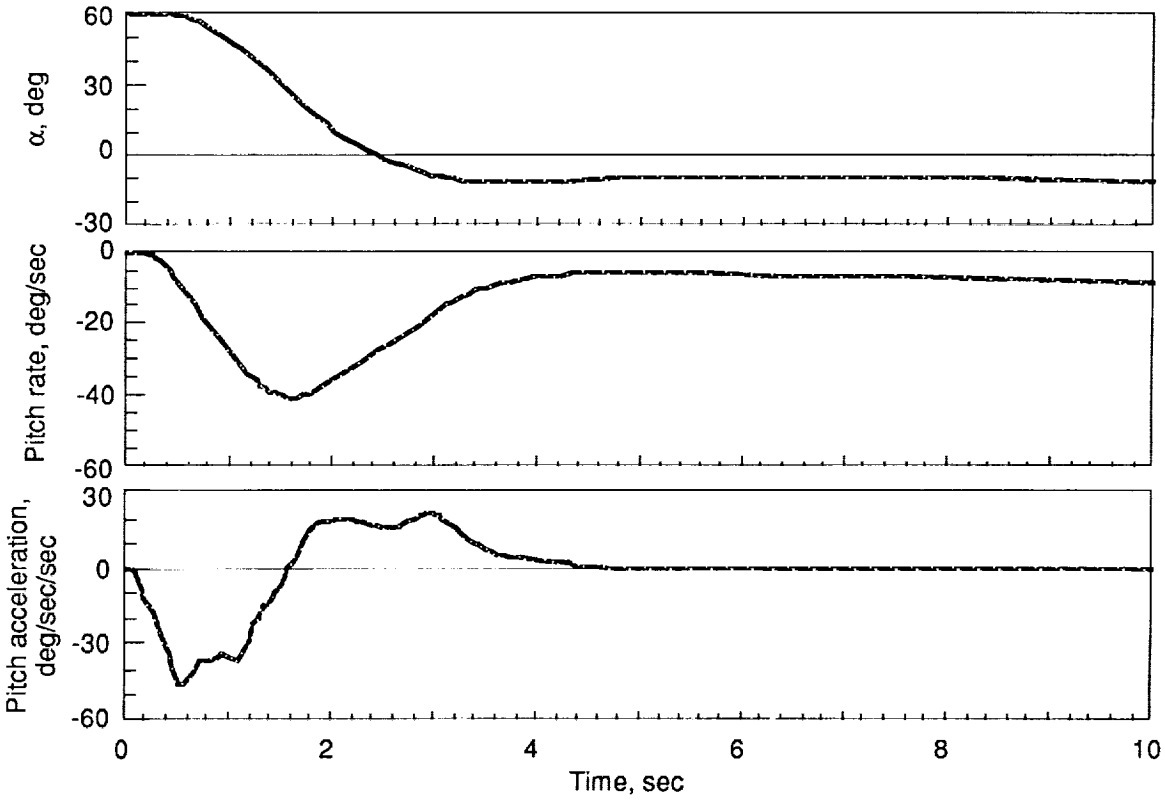

Figure 8. Pitch-down response, full forward stick at 25 000 ft.

of 45°, the stabilator (not shown) was saturated trailing edge down at approximately 6.2 sec and the pitch thrust-vectored command was quite close to saturation.

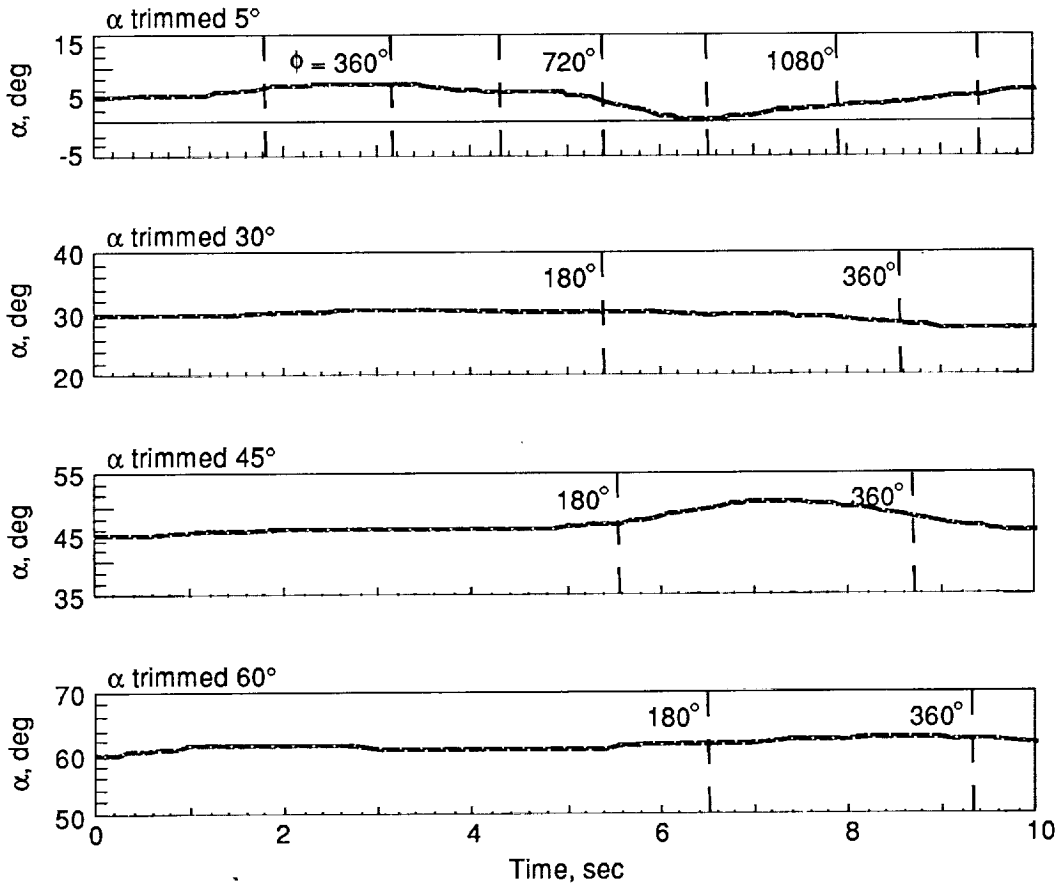

Figure 9. Angle-of-attack regulation, full lateral stick roll at 25 000 ft.

Conclusions

This paper presents the methodology used to design a longitudinal controller for a high-angle-of-attack aircraft that operates in a highly nonlinear flight regime deep into the poststall regime. The paper covers information such as theoretical development, control guidelines, design application, and results. Mathematical formulations for both variable-gain output feedback and the proportional integral filter control structure were described, followed by a summary of appropriate longitudinal control design guidelines for flight at a high angle of attack (α). The design approach for the feedback controller includes an approximate design procedure for determination of the starting point and for adjustment of the optimal weights. A description of the design approach for the feed-forward controller was also included. Finally, linear analysis results and nonlinear batch simulation examples were described. Based upon the design and application results, the following conclusions can be made:

1. The use of established relationships to adjust the optimal weights allows the designer to make trade-offs between control power, errors in regulated variables, bandwidth of the control filter, and phase lag. Such adjustments work well in the design process.

2. The derivation of the feed-forward command generator illustrates a good blending procedure between the load-factor command mode and α command mode; the transition between these command modes is undetectable in the time responses. The derivation also shows good

integration between the feedback and feed-forward controllers, which is demonstrated by the smooth response shown in the nonlinear simulation results.

3. Of 133 test conditions, all cases in the flight envelope meet the guidelines for both the 6-dB gain margin and the 45°-phase margin. In addition, except for a few high-speed cases at 15 000 ft, all other test cases outside the flight envelope also meet these guidelines.

4. The filter in the PIF control structure provides additional attenuation to help meet the servoelastic guidelines. The peak structural frequency at 100 rad/sec is attenuated to at least −20 dB, which is significantly better than the guideline of −8 dB.

5. A μ analysis was performed for multiplicative errors at the plant output and for sensitivity evaluations of multiplicative errors in stability and control derivatives. This analysis indicates a reasonably robust control system. Analysis of four stability derivatives for the 39 design cases shows the minimum singular values (with one exception) above 1 for the frequency range near the short period; results for four control derivatives show all minimums above 0.6. Although no concrete guidelines have been established for this type of analysis, these minimums are quite good.

6. Nonlinear batch simulations demonstrate good agility in both pitch-up and pitch-down full-stick maneuvers. Both the pitch-rate and pitch-acceleration responses are much better than the agility guidelines for the pitch-down maneuver. For the pitch-up maneuver, the pitch acceleration is slightly greater than the guideline, whereas the pitch-rate peak is slightly below the agility guideline. In addition, results of four trim conditions from low to high α show that α regulation is very good and exceeds the guideline for all cases.

7. The variable-gain methodology is practical for high-α applications. Incorporation of an internally generated, optimal gain schedule, using a priori selected gain schedule measurements, allows for an integrated design that is accomplished in a single process. This design approach is more efficient than classical methods that use a separate design for each operating condition.

8. The PIF control structure and its incremental implementation are shown to work well in a nonlinear environment. The controller is a direct digital formulation that accommodates the computational time lag from rate command to position command. Control of the rate command can ensure that actuators are not overdriven. The incremental implementation means that sensor biases are subtracted out of the proportional feedback loop. In the integrator loop, the pilot can move the pitch stick slightly to compensate for biases. The command-generator tracker feed-forward gain allows changes in pilot commands to go directly to the rate command signal, which results in faster transient response.

NASA Langley Research Center
Hampton, VA 23681-0001
December 23, 1992

Appendix

Pitch-Rate Compensation

This appendix has two sections. The first section is a nomenclature list. The second section contains a derivation for pitch-rate compensation that draws from the definitions below.

Nomenclature

g	acceleration of gravity, ft/sec^2
K	constant
L	aerodynamic lift force, lb
m	mass, slugs
p	body-axis roll rate, deg/sec
p_s	stability-axis roll rate, deg/sec
q	body-axis pitch rate, deg/sec
q_{comp}	pitch-rate compensation, deg/sec
q_w	wind-axis pitch rate, deg/sec
r	body-axis yaw rate, deg/sec
T_{zw}	propulsive force along the normal wind axis
V	total airspeed, ft/sec
α	angle of attack, rad
$\dot{\alpha}$	time derivative of angle of attack, rad/sec
β	sideslip angle, rad
θ	body-axis pitch attitude angle, rad
θ_w	wind-axis pitch attitude angle, rad
ϕ	body-axis bank attitude angle, rad
ϕ_w	wind-axis bank attitude angle, rad

Derivation of Compensation

Start with the normal force equation of motion (ref. 11) in the wind axis at the aircraft center of gravity and use a flat Earth approximation to obtain

$$-mVq_w = T_{zw} - L + mg\cos\theta_w\cos\phi_w \tag{A1}$$

Use the definition of the wind-axis pitch rate q_w (ref. 11)

$$q_w = (q - \dot{\alpha})\cos\beta - (p\cos\alpha + r\sin\alpha)\sin\beta \tag{A2}$$

to obtain after substitution

$$mV\,(\dot{\alpha} - q)\cos\beta + mVp_s\sin\beta = T_{zw} - L + mg\cos\theta_w\cos\phi_w \tag{A3}$$

where the definition for stability-axis roll rate p_s is included as

$$p_s = p\cos\alpha + r\sin\alpha \tag{A4}$$

Redefine the wind-axis Euler angles in terms of body-axis Euler angles and angle of attack (α) as

$$\cos\theta_w\cos\phi_w = \sin\alpha\sin\theta + \cos\alpha\cos\theta\cos\phi \tag{A5}$$

Substitute into equation (A3) to obtain

$$mV\left(\dot{\alpha} - q\right)\cos\beta + mVp_s\sin\beta = T_{zw} - L + mg\left(\cos\theta\cos\phi\cos\alpha + \sin\theta\sin\alpha\right) \tag{A6}$$

Because we are solving for the nonlinear coupling terms that affect q, let the external forces (T_{zw} and L) be assumed at constant K and let $\dot{\alpha}$ be assumed as zero. This last assumption is used because the objective is to maintain α at trim during a stability-axis roll. The revised equation is

$$-Vq\cos\beta + Vp_s\sin\beta - g\left(\cos\theta\cos\phi\cos\alpha + \sin\theta\sin\alpha\right) = K \tag{A7}$$

Use small-angle assumptions for β and solve for q to yield

$$q = p_s\beta - \frac{g}{V}\left(\cos\theta\cos\phi\cos\alpha + \sin\theta\sin\alpha\right) - K \tag{A8}$$

where the first two terms on the right side of equation (A8) should be compensated. The pitch-rate compensation q_{comp} is

$$q_{\text{comp}} = \frac{g}{V}\left(\cos\theta\cos\phi\cos\alpha + \sin\theta\sin\alpha\right) - p_s\beta \tag{A9}$$

Use a constant value of 32.1 for the acceleration due to gravity (based upon an altitude range from 15 000 ft to 35 000 ft) and multiply the gravity compensation term by $180/\pi$ to obtain units in degrees per second. The yield is

$$q_{\text{comp}} = \frac{1839}{V}\left(\cos\theta\cos\phi\cos\alpha + \sin\theta\sin\alpha - 1\right) - p_s\beta \tag{A10}$$

where the -1 term is included to obtain a zero bias at the neutral stick position when ϕ and β are zero and the flight path angle is zero ($\theta = \alpha$).

References

1. Halyo, Nesim; Moerder, Daniel D.; Broussard, John R.; and Taylor, Deborah B.: *A Variable-Gain Output Feedback Control Design Methodology.* NASA CR-4226, 1989.

2. Halyo, Nesim: A Variable-Gain Output Feedback Control Design Approach. *A Collection of Technical Papers, Part 2—AIAA Guidance, Navigation and Control Conference,* Aug. 1989, pp. 1238–1248. (Available as AIAA-89-3575-CP.)

3. Moerder, Daniel D.; Halyo, Nesim; Broussard, John R.; and Caglayan, Alper K.: Application of Precomputed Control Laws in a Reconfigurable Aircraft Flight Control System. *J. Guid., Control, & Dyn.,* vol. 12, May–June 1989, pp. 325–333.

4. Ostroff, Aaron J.: High-Alpha Application of Variable-Gain Output Feedback Control. *J. Guid., Control, & Dyn.,* vol. 15, Mar. Apr. 1992, pp. 491–497.

5. Broussard, John R.: *Design, Implementation and Flight Testing of PIF Autopilots for General Aviation Aircraft.* NASA CR-3709, 1983.

6. Maybeck, Peter S.: *Stochastic Models, Estimation, and Control, Volume 3.* Academic Press, 1982.

7. Broussard, John R.; and O'Brien, Mike J.: Feedforward Control To Track the Output of a Forced Model. *IEEE Trans. Autom. Control,* vol. AC-25, no. 4, Aug. 1980, pp. 851–853.

8. Forster, John V.; Bundick, W. T.; and Pahle, Joseph W.: Controls for Agility Research in the NASA High-Alpha Technology Program. SAE Paper 912148, Sept. 1991.

9. *Military Specification—Flight Control System—General Specification For.* MIL-F-87242 (USAF), U.S. Air Force, Mar. 31, 1986.

10. Doyle, John: Analysis of Feedback Systems With Structured Uncertainties. *IEE Proc.,* vol. 129, pt. D, no. 6, Nov. 1982, pp. 242–250.

11. Etkin, Bernard: *Dynamics of Atmospheric Flight.* John Wiley & Sons, Inc., c.1972.

REPORT DOCUMENTATION PAGE

Form Approved
OMB No. 0704-0188

1. AGENCY USE ONLY(Leave blank)	2. REPORT DATE	3. REPORT TYPE AND DATES COVERED
	February 1993	Technical Paper

4. TITLE AND SUBTITLE
Longitudinal-Control Design Approach for High-Angle-of-Attack Aircraft

5. FUNDING NUMBERS
WU 505-64-30-01

6. AUTHOR(S)
Aaron J. Ostroff and Melissa S. Proffitt

7. PERFORMING ORGANIZATION NAME(S) AND ADDRESS(ES)
NASA Langley Research Center
Hampton, VA 23681-0001

8. PERFORMING ORGANIZATION REPORT NUMBER
L-17123

9. SPONSORING/MONITORING AGENCY NAME(S) AND ADDRESS(ES)
National Aeronautics and Space Administration
Washington, DC 20546-0001

10. SPONSORING/MONITORING AGENCY REPORT NUMBER
NASA TP-3302

11. SUPPLEMENTARY NOTES
Ostroff: Langley Research Center, Hampton, VA; and Proffitt: Lockheed Engineering & Sciences Co., Hampton, VA.

12a. DISTRIBUTION/AVAILABILITY STATEMENT
Unclassified Unlimited

Subject Category 08

12b. DISTRIBUTION CODE

13. ABSTRACT *(Maximum 200 words)*

This paper describes a control synthesis methodology that emphasizes a variable-gain output feedback technique that is applied to the longitudinal channel of a high-angle-of-attack aircraft. The aircraft is a modified F/A-18 aircraft with thrust-vectored controls. The flight regime covers a range up to a Mach number of 0.7; an altitude range from 15 000 to 35 000 ft; and an angle-of-attack (α) range up to 70°, which is deep into the poststall region. A brief overview is given of the variable-gain mathematical formulation as well as a description of the discrete control structure used for the feedback controller. This paper also presents an approximate design procedure with relationships for the optimal weights for the selected feedback control structure. These weights are selected to meet control design guidelines for high-α flight controls. Those guidelines that apply to the longitudinal-control design are also summarized. A unique approach is presented for the feed-forward command generator to obtain smooth transitions between load factor and α commands. Finally, representative linear analysis results and nonlinear batch simulation results are provided.

14. SUBJECT TERMS	15. NUMBER OF PAGES
Longitudinal control; High α; Variable gain; Feedback control; Feed-forward control; Airplane control; Aircraft control	28
	16. PRICE CODE A03

17. SECURITY CLASSIFICATION OF REPORT	18. SECURITY CLASSIFICATION OF THIS PAGE	19. SECURITY CLASSIFICATION OF ABSTRACT	20. LIMITATION OF ABSTRACT
Unclassified	Unclassified		

NSN 7540-01-280-5500

Standard Form 298(Rev. 2-89)
Prescribed by ANSI Std. Z39-18
298-102

NASA-Langley, 1993